Differential Photoelectron Holography: A New Approach for Three-Dimensional Atomic Imaging

S. Omori,[1,2] Y. Nihei,[1] E. Rotenberg,[3] J. D. Denlinger,[3] S. Marchesini,[2] S. D. Kevan,[4] B. P. Tonner,[5] M. A. Van Hove,[2,3,6] and C. S. Fadley[2,6]

[1]*Institute of Industrial Science, University of Tokyo, Tokyo 153-8505, Japan*
[2]*Materials Sciences Division, Lawrence Berkeley National Laboratory, Berkeley, California 94720*
[3]*Advanced Light Source, Lawrence Berkeley National Laboratory, Berkeley, California 94720*
[4]*Department of Physics, University of Oregon, Eugene, Oregon 97403*
[5]*Department of Physics, University of Central Florida, Orlando, Florida 32816*
[6]*Department of Physics, University of California, Davis, California 95616*

(Received 31 October 2000; published 17 January 2002)

We propose differential holography as a method to overcome the long-standing forward-scattering problem in photoelectron holography and related techniques for the three-dimensional imaging of atoms. Atomic images reconstructed from experimental and theoretical Cu $3p$ holograms from Cu(001) demonstrate that this method suppresses strong forward-scattering effects so as to yield more accurate three-dimensional images of side- and backscattering atoms.

DOI: 10.1103/PhysRevLett.88.055504 PACS numbers: 61.14.–x, 42.40.–i

Holography [1] is a method of recording both the amplitudes and phases of waves scattered by an object illuminated with coherent radiation, and using this information to directly construct a three-dimensional image of the object. Szöke [2] first suggested that coherent outgoing waves from atomically localized sources of photoelectrons, fluorescent x rays, and γ rays could be used to achieve atomic-scale holography. This idea was initially demonstrated theoretically for the case of photoelectrons by Barton [3], and then extended into a multienergy format by Barton and Terminello and by Tong and co-workers [4]. By now several experimental approaches to such atomic-resolution holography have been demonstrated, including photoelectrons [5–8], Auger electrons [9], Kikuchi electrons [10], diffuse-scattered low-energy electrons [11], fluorescent x rays in either a direct mode [12] or a multienergy inverse mode [13], γ rays [14], and bremsstrahlung x rays [15].

Among these methods, photoelectron holography (PH) has the advantages of being capable of studying the local atomic structure around each type of emitter without requiring long-range order and of distinguishing emitters through core-level binding-energy shifts [8]. Photoelectron holograms also show strong modulations of up to $\pm 50\%$, so such effects are easily measurable. However, PH can suffer from serious image aberrations due to the strength of electron scattering. The atomic scattering factor f is a highly anisotropic function of scattering angle, and can depend strongly on electron kinetic energy E_k. In particular, as E_k increases above a few hundred eV, f becomes more and more significant in the forward direction, resulting in a strong forward-scattering (FS) peak [16] that can induce image aberrations. Beyond this, PH also can suffer from multiple-scattering (MS) effects due to the scattering strength.

Various reconstruction algorithms and measurement methods [4,5,7,17] have been proposed to correct for the anisotropic f and MS effects, some of which can be summarized via

$$U(\mathbf{r}) = \left| \int W(\mathbf{r}, \mathbf{k}) \chi(\mathbf{k}) \exp[-ikr + i\mathbf{k} \cdot \mathbf{r}] \, d^3\mathbf{k} \right|^2, \tag{1}$$

where U is the image intensity at position $\mathbf{r}$, χ is the normalized 3D hologram, and the function or operator W permits describing the difference between algorithms, with $W = 1$ in the original multienergy formulations [4]. One alternative algorithm [5] sets $W = f^{-1}(k, \theta_{\mathbf{r}}^{\mathbf{k}})$ so as to divide out the anisotropic f, where $\theta_{\mathbf{r}}^{\mathbf{k}}$ is the angle between $\mathbf{r}$ and $\mathbf{k}$. In another algorithm [7] based on the more ideal electron backscattering (BS), a window function for W that limits the integral in Eq. (1) to be in a small cone of $\hat{\mathbf{k}}$ around $-\mathbf{r}$ is chosen to emphasize the imaging of BS atoms. Although successful in several applications [7,18], it is difficult to apply this small-cone method to many systems where the imaging of FS or even side-scattering (SS) atoms is important, such as epitaxial films and buried interfaces. In fact, imaging of "bulk" atoms surrounded by FS and BS atoms via PH has proven to be especially difficult (cf. Figs. 7–9 in Ref. [8]), with most successful applications being to emitters in the first few layers near a surface.

To overcome such FS effects, we propose in this Letter "differential holography." By simply replacing χ in Eq. (1) by its k derivative (i.e., $W = \partial/\partial k$) or more conveniently by a numerical difference between two χ's at different energies [$\delta\chi = \chi(k + \delta k) - \chi(k)$], FS effects can be greatly suppressed. We have applied this method to multienergy holograms for Cu $3p$ emission from Cu(001), and show that this provides images that are improved over prior work in several respects.

To avoid confusion with other methods in PH, we also note that "derivative" PH has been proposed and used successfully by Luh and co-workers [18]. However, the purpose here is to eliminate uncertainties in I due to the variation of experimental conditions by first taking logarithmic derivatives $[\partial I/\partial k]/I$ that are then reintegrated into "self-normalized" intensities; thus, it is still finally χ that is used in Eq. (1).

The principle of differential photoelectron holography (DPH) is as follows. We consider the single-scattering expression of χ for an emitter-scatterer pair spaced by a vector $\mathbf{r}$ [16]:

$$\chi(\mathbf{k}) = \frac{I - I_0}{I_0} \approx \frac{2|f(k,\theta_{\mathbf{r}}^{\mathbf{k}})|}{r}\cos[kr(1-\cos\theta_{\mathbf{r}}^{\mathbf{k}}) + \varphi(k,\theta_{\mathbf{r}}^{\mathbf{k}})], \quad (2)$$

where I_0 is the intensity that would be observed without atomic scattering, and φ is the scattering phase. If δk is sufficiently small so that $\delta|f|/|f| \ll 1$, where $\delta|f|$ is the change in $|f|$, the difference of two holograms at $k_\pm = k \pm \delta k/2$ can be written in a similar form to Eq. (2) as

$$\delta\chi(\mathbf{k}) = \chi(k_+\hat{\mathbf{k}}) - \chi(k_-\hat{\mathbf{k}}) \approx -\frac{2|f_{\text{eff}}|}{r}\sin[kr(1-\cos\theta_{\mathbf{r}}^{\mathbf{k}}) + \bar{\varphi}(k,\theta_{\mathbf{r}}^{\mathbf{k}})], \quad (3)$$

where direction $\hat{\mathbf{k}}$ is defined by angles θ and ϕ, the "effective" scattering amplitude is defined as $|f_{\text{eff}}| = 2|f|\sin[\delta kr(1-\cos\theta_{\mathbf{r}}^{\mathbf{k}})/2 + \delta\varphi/2]$, and $\bar{\varphi}$ is the average of φ's at $k_\pm$. In the FS region where $\theta_{\mathbf{r}}^{\mathbf{k}} \to 0$, $|f_{\text{eff}}|$ is thus very small, approaching zero in the limit of $\delta\varphi \to 0$. If δk is also small, $|f_{\text{eff}}|$ is proportional to r; thus, DPH not only suppresses the FS effects, but also enhances the imaging of distant atoms. In Fig. 1, $|f|$ and $|f_{\text{eff}}|$ are plotted as a function of $\theta_{\mathbf{r}}^{\mathbf{k}}$ for Cu-Cu nearest neighbors ($r = 2.56$ Å). For $k = 4.6$ Å^{-1} and $\delta k = 0.2$ Å^{-1}, $|f_{\text{eff}}|$ is significant only in the region of $\theta_{\mathbf{r}}^{\mathbf{k}} > \sim 90°$. Therefore, the imaging of SS and BS atoms is expected, while it will be difficult for this case to image FS atoms. On the other hand, for $k = 8.8$ Å^{-1} and a larger fractional $\delta k = 1.0$ Å^{-1}, $|f_{\text{eff}}|$ is significant not only in the BS region but also in the range of $\theta_{\mathbf{r}}^{\mathbf{k}} \sim 30°$–$90°$. Since near-neighbor FS diffraction fringes extend out beyond 30° [16,19], we might expect the latter choice to also permit imaging FS atoms. In this way, the relative sensitivity of DPH to SS and FS atoms can be "tuned" by selecting the range and step width of k scans. Finally, we note that the suppression of MS effects by means of a transform over a volume in $\mathbf{k}$ space is well known in normal multienergy PH [4] and this suppression will be equally present in DPH. If anything, the inherent elimination of strong FS effects in DPH should lead to even better MS suppression.

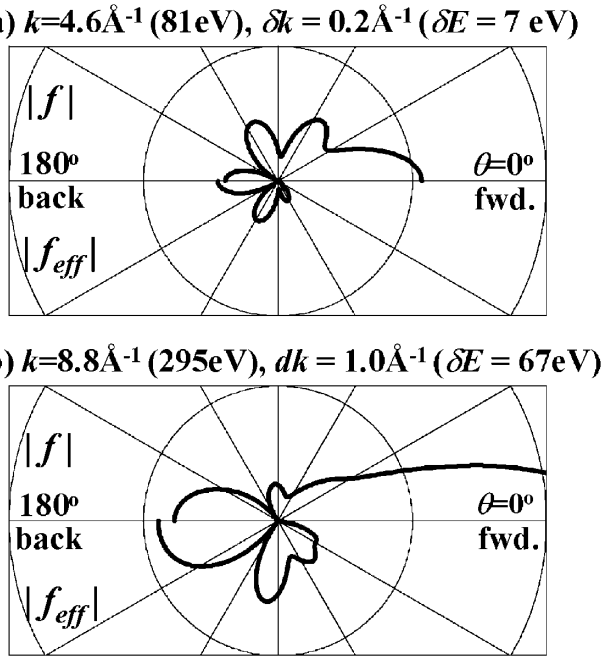

FIG. 1. Comparison of the usual scattering amplitude $|f|$ and the effective scattering amplitude of differential holography $|f_{\text{eff}}|$, calculated for Cu-Cu nearest neighbors ($r = 2.56$ Å) as a function of scattering angle $\theta_{\mathbf{r}}^{\mathbf{k}}$ for two different sets of k and δk in taking the differential of χ: (a) $k = 4.6$ Å^{-1} (81 eV), $\delta k = 0.2$ Å^{-1} (7 eV) and (b) $k = 8.8$ Å^{-1} (295 eV), $\delta k = 1.0$ Å^{-1} (67 eV). The final strong forward-scattering data points of $|f|$ at the right of panel (b) are truncated.

To demonstrate DPH experimentally, photoelectron holograms from Cu(001) were measured at beam line 7.0 of the Advanced Light Source at the Lawrence Berkeley National Laboratory. Photoelectron spectra for Cu $3p$ emission were collected at 25 energies over $k = 4.5$–9.3 Å^{-1} ($E_k = 77$–330 eV) with a constant step of $\delta k = 0.2$ Å^{-1} ($\delta Ek = 7$–14 eV), along 65 different directions over a symmetry-reduced 1/8 of the total solid angle above the specimen, and with a polar angle range from $\theta = 0°$ (surface normal) to 70°. The photoelectron intensity $I(k,\theta,\phi)$ was fitted by low-order polynomials to obtain the smooth background intensity [8,20]:

$$I_0(k,\theta) = (a_0 + a_1k + a_2k^2) \times (b_0 + b_1\cos\theta + b_2\cos 3\theta). \quad (4)$$

Three kinds of χ were obtained from this fitting: χ_A by fitting the second factor of Eq. (4) to a scanned-angle pattern $I_k(\theta,\phi)$ at each fixed k [6], χ_B by fitting the first factor to a scanned-energy curve $I_{\hat{\mathbf{k}}}(k)$ at each fixed direction $\hat{\mathbf{k}}$ [7], and χ_C by fitting both factors to the full data set of $I(k,\theta,\phi)$ at one time, with the last expected to be the most accurate from an *a priori* point of view [8]. The k differences from χ_C were also used for DPH in what we will term method D (i.e., $\chi_D = \delta\chi_C$). Since low-frequency fringes due to FS events in $I_{\hat{\mathbf{k}}}(k)$ are automatically removed in method B [10], the resulting I_0 inherently

deviates from the true I_0 defined as the intensity without scattering, especially in the FS direction. In addition, since $I_k(\theta,\phi)$ and $I_{\hat{\mathbf{k}}}(k)$ are independently normalized without considering the continuity of χ in the whole sampled $\mathbf{k}$ space in methods A and B, they could degrade holographic fringes in $I_{\hat{\mathbf{k}}}(k)$ and $I_k(\theta,\phi)$, respectively. By contrast, method C takes into account the continuity of χ over the whole data set, but the FS peaks remain in χ_C; however, they should be eliminated in χ_D. The original transform of Eq. (1) was used for all four data sets; but to avoid the abrupt truncation of the integral in Eq. (1), W was taken to be the product of a Gaussian function of k and a Hanning function $\cos^2\theta$, with an additional multiplication by r to make atoms at larger distances more visible.

Figure 2 shows atomic images reconstructed from $\chi_A - \chi_D$ in the vertical (100) plane of Cu(001). In methods A and C, only elongated features related to FS effects from atoms of types 6 and 7 are observed above $z_c = -0.5$ Å (the arbitrary location of a change in image multiplication). This is consistent with a previous PH study of W(110) [8], in which method C was used. By contrast, it has been reported [6] that FS atoms of type 5 have been imaged via method A from Cu $3p$ holograms for Cu(001) obtained at nine energies. Even if possible differences in the two sets of experimental data are taken into account, it is difficult to conclude from our results that the images of these FS atoms can be resolved from strong artifacts via method A. Below z_c, several peaks near the BS positions 1–3 are observable for A and C among various strong artifacts, but only with the help of higher image amplifications of 46 and 29, respectively.

In methods B and D, image intensities are stronger in the BS region, with the relative image amplification factors being reversed in sense and smaller at ×5 compared to A and C. In method D, a strong, somewhat elongated peak is observed at the FS position 6, with weaker features that appear to be associated with atoms 7 also present in the corners of the image. In both B and D, two strong peaks are observed at the SS positions 4 above z_c and five peaks are observed at the BS positions 1–3 below z_c. However, the most intense features in method B are the artifacts between the two nearest BS atoms of type 3. In method D, by contrast, the five strongest peaks below z_c are of roughly equal intensity and correspond reasonably well to the near-neighbor BS atoms. Therefore, we find method D to be the most robust for imaging both SS and BS atoms (as well as to some degree also FS atoms 6), even if there are shifts in position of approximately 0.1 Å for type 1, 0.6 Å for 2, and 0.3 Å for 3. Such peak shifts relative to the true atomic positions, as observed in all methods, can be attributed to the present neglect of corrections for both the scattering phase and the inner potential.

For comparison with experiment, we have also performed MS simulations of $I(\mathbf{k})$, using a cluster method fully described elsewhere [21]. The theoretical I_0 was obtained simply as the square of the zeroth-order wave function without scattering. Images reconstructed from the theoretical χ and $\delta\chi$ via methods C and D are shown in Figs. 2(e) and 2(f) and can be compared with Figs. 2(c) and 2(d), respectively. The main features in Figs. 2(c) and 2(d) are well reproduced by our simulations, although the artifacts between the atoms 3 are much stronger in experiment for C, and the relative intensity in the region of FS atom 6 is stronger in experiment for D. Even though the ideal χ was used for image reconstruction, no atomically

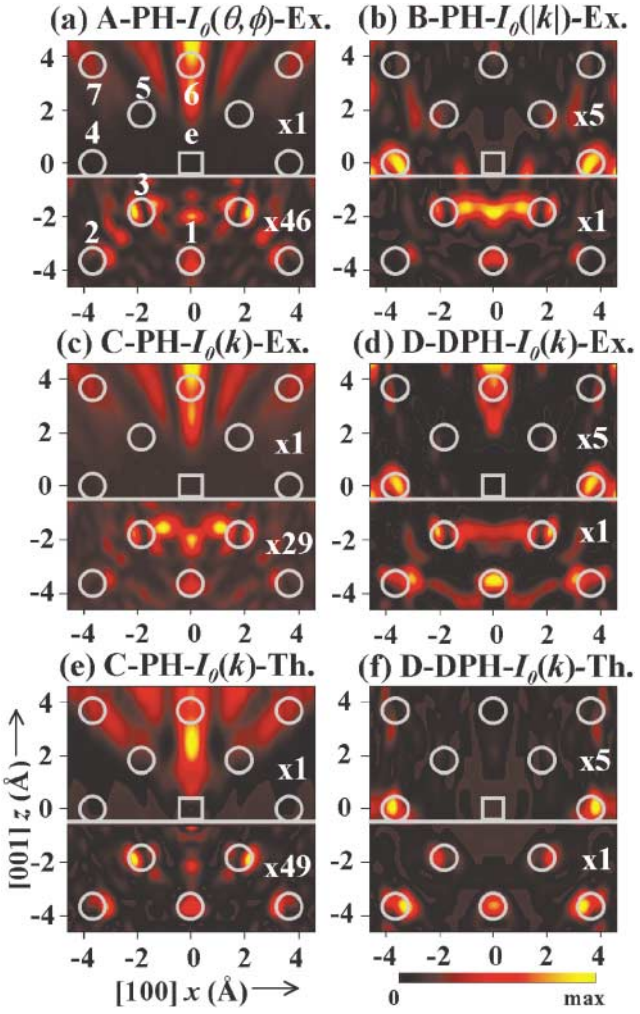

FIG. 2 (color). Atomic images in the vertical (100) plane of Cu (001) reconstructed from Cu $3p$ holograms obtained by methods A–D, as described in the text. The emitter and scatterer positions are indicated by squares and circles, respectively, and various near-neighbor atoms are numbered. Image intensities above or below $z_c = -0.5$ Å have been rescaled by the factor shown in each panel, with this factor being determined so as to make the maximum intensities above and below z_c equal. Experimental images (a) Image from method A: normal holography with I_0 determined by fitting the angular variation of Eq. (4) at each k value. (b) Image from method B: normal holography with I_0 determined by fitting the k variation along each direction. (c) Image from method C: normal holography with I_0 determined by fitting both the angular and k variation. (d) Image from method D: differential holography, with I_0 as in (c). Theoretical images: (e) As (c) but theoretical.

resolved SS or FS peaks are observable in Fig. 2(e). Therefore, the corresponding artifacts in Fig. 2(c) are not purely due to the uncertainties in the experimental data and any errors in the I_0 subtraction, but must have their origin in the MS effects and basic imaging algorithm. On the other hand, Fig. 2(f) exhibits well-resolved peaks at the SS and BS positions. Since there are no artifacts below z_c in Fig. 2(f), the artifacts in Fig. 2(d) are by contrast considered to be purely due to the experimental noise and other nonidealities in the data analysis.

We have also generated full three-dimensional atomic images from the experimental data via χ_D, although length limitations prevent showing these here. In these images, we find in addition to the atoms 1–4 and 6 in Fig. 2, two other types of near-neighbor BS and SS atoms located in the vertical (110) plane (denoted types $2'$ and $4'$ and situated in the same horizontal layers as 2 and 4, respectively). All of these atoms are reasonably well reconstructed, with only a few, such as 2, being significantly shifted in position, but most within a few tenths of an Å of the correct positions in all directions. The overall positional errors for all of the atoms compared to the known Cu lattice can be summarized as (radial location shift in xy)/(vertical location shift in z), and are 0.0 Å/0.1 Å for atoms 1, 0.6 Å/0.1 Å for 2, 0.3 Å/0.1 Å for $2'$, 0.2 Å/0.1 Å for 3, 0.1 Å/0.0 Å for 4, 0.3 Å/0.0 Å for $4'$, and 0.0 Å/0.4 Å for 6. As a further indication of the overall image quality obtained by DPH, the reader is referred to an animated comparison of 3D images for the four approaches of Figs. 2(a)–2(d), in which DPH is alone in imaging approximately 15 near-neighbor atoms [22].

Finally, we compare DPH with a very recently introduced approach for PH termed near-node holography [23], in which FS effects are suppressed by using a special experimental geometry with electron exit nearly perpendicular to light polarization. Although this technique is promising, DPH has the advantages that it does not require a special experimental geometry or s-subshell-like form for the photoelectric cross section, that it seems to yield images of as good or better quality [22,23], and that it can be used in other types of holography in which polarization cannot be varied.

In summary, we have demonstrated differential photoelectron holography (DPH) as a powerful method for overcoming the FS problem in PH and enhancing image quality for any kind of system in which FS can arise, as, for example, bulk emission and buried interfaces. This method should also be helpful in other types of electron holography in which energy can be stepped in a controlled way (e.g., Kikuchi [10] or LEED [11] holography). The reconstructed images for Cu $3p$/Cu(001) demonstrate that DPH is successful in suppressing the FS effects so as to image SS, BS, and to some degree also FS, atoms with accuracies of 0.1–0.6 Å.

This work was supported in part by the Director, Office of Energy Research, Basic Energy Science, Materials Sciences Division of the U.S. Department of Energy under Contract No. DE-AC03-76SF00098. S. O. and Y. N. also acknowledge the support of the Japan Society for the Promotion of Science (Grant No. JSPS-RFTF 98R14101).

[1] D. Gabor, Nature (London) **161**, 777 (1948).
[2] A. Szöke, in *Short Wavelength Coherent Radiation: Generation and Applications,* edited by D. T. Attwood and J. Boker, AIP Conf. Proc. No. 147 (AIP, New York, 1986), p. 361.
[3] J. J. Barton, Phys. Rev. Lett. **61**, 1356 (1988).
[4] J. J. Barton, Phys. Rev. Lett. **67**, 3106 (1991); J. J. Barton and L. J. Terminello, in *Structure of Surfaces III,* edited by S. Y. Tong, M. A. Van Hove, X. Xide, and K. Takayanagi (Springer-Verlag, Berlin, 1991), p. 107; S. Y. Tong, H. Li, and H. Huang, Phys. Rev. Lett. **67**, 3102 (1991).
[5] B. P. Tonner *et al.,* Phys. Rev. B **43**, 14 423 (1991).
[6] L. J. Terminello, J. J. Barton, and D. A. Lapiano-Smith, Phys. Rev. Lett. **70**, 599 (1993).
[7] S. Y. Tong, H. Li, and H. Huang, Phys. Rev. B **51**, 1850 (1995); H. Wu and G. J. Lapeyre, *ibid.* **51**, 14 549 (1995).
[8] P. M. Len *et al.,* Phys. Rev. B **59**, 5857 (1999).
[9] D. K. Saldin, G. R. Harp, and X. Chen, Phys. Rev. B **48**, 8234 (1993).
[10] C. M. Wei, I. H. Hong, and Y. C. Chou, Surf. Rev. Lett. **1**, 335 (1994).
[11] D. K. Saldin and P. L. DeAndres, Phys. Rev. Lett. **64**, 1270 (1990); K. Reuter *et al.,* Phys. Rev. B **58**, 4102 (1998).
[12] M. Tegze and G. Faigel, Europhys. Lett. **16**, 41 (1991); P. M. Len *et al.,* Phys. Rev. B **50**, 11 275 (1994).
[13] T. Gog *et al.,* Phys. Rev. Lett. **76**, 3132 (1996).
[14] P. Korecki, J. Korecki, and T. lezak, Phys. Rev. Lett. **79**, 3518 (1997).
[15] S. G. Bompadre, T. W. Petersen, and L. B. Sorensen, Phys. Rev. Lett. **83**, 2741 (1999).
[16] C. S. Fadley, Surf. Sci. Rep. **19**, 231 (1993).
[17] T. Greber and J. Osterwalder, Chem. Phys. Lett. **256**, 653 (1996).
[18] D.-A. Luh, T. Miller, and T.-C. Chiang, Phys. Rev. Lett. **81**, 4160 (1998).
[19] S. Omori, T. Kozakai, and Y. Nihei, Surf. Rev. Lett. **6**, 1085 (1999).
[20] P. M. Len, Ph.D. thesis, University of California, Davis, 1997.
[21] Y. Chen *et al.,* Phys. Rev. B **58**, 13 121 (1998); multiple scattering photoelectron diffraction program at http://electron.lbl.gov/mscdpack/mscdpack.html.
[22] See AIP Document No. EPAPS: E-PRLTAO-88-029206 for an animated comparison of 3D images for the four approaches of Figs. 2(a)–2(d). This document may be retrieved via the EPAPS homepage (http://www.aip.org/pubservs/epaps.html) or from ftp.aip.org in the directory /epaps/. See the EPAPS homepage for more information. Similar images also appear at http://electron.lbl.gov/marchesini/dph.
[23] J. Wider *et al.,* Phys. Rev. Lett. **86**, 2337 (2001).